Quadrotors & Accelerometers

State Estimation with an Improved Dynamic Model

Robert C. Leishman, John Macdonald, Randal W. Beard, Timothy W. McLain

Quadrotors are ideal platforms for autonomous flight in unknown and complex environments. Their small size and maneuverability are conducive to operating in confined spaces and avoiding obstacles. Equipped with appropriate sensors and algorithms, quadrotors could enable several applications currently infeasible for ground robots.

A quadrotor's small size and maneuverability also create problems for making them autonomous. The same fast dynamics that make quadrotors maneuverable require accurate and frequently updated position, orientation, and velocity state estimates to enable autonomous control. Additionally, the amount of energy and payload available on a quadrotor limits the available sensors and processing capability. These problems are especially relevant in unknown and complex 3D environments that demand more processing-intensive algorithms and information-rich sensor data.

A few research groups have made noteworthy progress toward deploying fully autonomous quadrotors. The authors of [1] present their system while noting that one of the major challenges is estimating the position and velocity. To address this problem they develop a sophisticated laser scan-matching algorithm. They characterize that algorithm as the key

technology that allows their vehicle to fly.

In [2] the authors present a quadrotor system also using a scanning laser rangefinder. They state that the fast vehicle dynamics require pose estimates with update rates of 20 Hz. Several of their design decisions are driven by the need to meet the system's computational limitations.

The authors of [3] rely on the increased information available from cameras at the expense of increased computation. They emphasize that the estimated velocity is critical to damp the system. Their estimator relies on a simple constant-velocity motion model that raises the minimum update rate the filter requires from the vision processing.

It is clear that accurate and timely state estimates, of attitude and velocity in particular, are key ingredients to enable an autonomous quadrotor. In this article, we present results showing how velocity and attitude estimates can benefit from an improvement to the traditional quadrotor dynamic model.

An assumption of the widely-used (e.g. [4]–[11]) traditional quadrotor model is that the only significant forces acting on the vehicle are gravity and the thrust produced by the rotors (see Figure 1). This assumption leads to a dynamic model for the quadrotor's linear acceleration given by

$$\begin{bmatrix} \dot{u} \\ \dot{v} \\ \dot{w} \end{bmatrix} = \mathbf{R}_I^b \begin{bmatrix} 0 \\ 0 \\ g \end{bmatrix} - \begin{bmatrix} 0 \\ 0 \\ \frac{T}{m} \end{bmatrix}, \tag{1}$$

where $\dot{u}$, $\dot{v}$, and $\dot{w}$ are the components of acceleration along the body-fixed $\vec{i}_b$, $\vec{j}_b$, and $\vec{k}_b$ axes, as shown in Figure 1. $\mathbf{R}_I^b$ is the rotation matrix from the inertial to the body-fixed reference

frame. The constants g and m represent the gravitational acceleration and the quadrotor's mass. The combined thrust of the rotors is T and is an input to the system.

This model is acceptable for some applications, such as designing a controller, because it captures the external forces with the most significant magnitudes. However, it leads to an interesting paradox that was articulated in [12]. The model implies accelerometers aligned with the $\vec{i}_b$ and $\vec{j}_b$ axes will always measure zero. Yet many successful quadrotor implementations using this model also use the accelerometer measurements to effectively improve estimates of the quadrotor's orientation.

An improved quadrotor model should explain how to more appropriately use the data from the accelerometers aligned with the $\vec{i}_b$ and $\vec{j}_b$ axes. Many papers acknowledge that some drag force must act on the vehicle's body, but this is reasonably dismissed as being small as it is proportional to the square of the vehicle's linear velocity. Other researchers include a drag force that is directly proportional to the quadrotor's linear velocity. For example, [13], [14], [15] and [16] identify similar terms. However, the authors' emphasis on control algorithms avoids any discussion of the physics that generate the drag or its effect on accelerometers or the state estimation process. A drag force proportional to linear velocity is included in the estimation approach of [1] based on the authors' observation that something must prevent the quadrotor from accelerating indefinitely. They too offer no physical explanation for the effect and instead rely on a motion capture system to estimate the proportionality constant.

Both [12] and [17] identify a term called *rotor drag* as the force acting in the body-fixed $\vec{i}_b$ and $\vec{j}_b$ axes. Reference [12] derives a dynamic model of the quadrotor based on concepts of fundamental blade-element theory, and they identify the rotor drag with the accelerometer

measurements. They conclude with a discussion of two controllers based on their drag-force-enhanced model. However, the resulting hardware implementations are only assessed qualitatively by stating that the systems were much easier to fly than with the usual scheme.

In this article we discuss how accelerometer measurements in quadrotor flight lead to improved estimation performance. We confirm, using hardware and truth data, that the accelerometers directly measure the translational velocity, allowing more accurate estimates of the attitude and velocity of the vehicle than can be achieved with traditional methods. In the "Accelerometer Tutorial" (sidebar) we lay the groundwork to explain why accelerometers in quadrotor flight measure the rotor drag. In many publications, like [3], [11], [18] for example, a subtle mistake is made when relating gravity to the accelerometer measurements on a quadrotor. In this article, we clarify this issue and show the agreement between the improved accelerometer model and actual measurements.

We also show how easy it is to use this new, drag-force-enhanced model. The drag force constant can be estimated as a state in a filter driven only by IMU measurements, thus removing the need for experimental tuning as in [12] or an expensive motion capture system as in [1]. We present several filters designed to work with only IMU measurements. We compare estimates to truth as well as estimates from more traditional approaches to quantify the benefit of the enhanced model in state estimation. In the results we show a twofold to threefold improvement in average attitude error compared to standard approaches.

We have used the drag-force-enhanced model that is introduced in this paper in other scenarios. Some preliminary analysis and a simplified application are presented in [19]. The benefits that the enhanced model provides to a filter that estimates position and yaw using

exteroceptive sensor measurements is discussed in [20].

Drag-force-enhanced Quadrotor Model

In this section we present a simplified version of the drag-force-enhanced model originally presented in [12]. We note here that this model applies equally well to any multirotor vehicle, not only quadrotors. We model the quadrotor with the nonlinear equations

$$\dot{\mathbf{x}} = \mathbf{f}(\mathbf{x}, \mathbf{u}) + \xi, \tag{2}$$

$$y_i = h_i(\mathbf{x}, \mathbf{u}) + \eta, i = 1, ..., p \tag{3}$$

where h_i is the i^{th} measurement function, and the vector $\mathbf{u}$ represents the inputs that drive the evolution of the estimated states. In this paper we will use the input

$$\mathbf{u} = \begin{bmatrix} p & q & r \end{bmatrix}^\top, \tag{4}$$

which are the rotation rates about the $\vec{i}_b$, $\vec{j}_b$, and $\vec{k}_b$ axes respectively and correspond to the outputs of the onboard gyroscopes after calibration. ξ and η are zero-mean Gaussian processes with covariance Q and R respectively.

With reference to Figure 1, the states we consider are

$$\mathbf{x} = \begin{bmatrix} \phi & \theta & \psi & u & v & w \end{bmatrix}^\top, \tag{5}$$

where ϕ, θ, and ψ are the Euler angles that relate the orientation of the body-fixed frame to the inertial frame, u, v, and w represent the components of linear velocity in the $\vec{i}_b$, $\vec{j}_b$, and $\vec{k}_b$ axes, respectively.

The drag-force-enhanced model is obtained from (1) by adding a drag force, which is proportional to the body-fixed-frame velocity, to the $\vec{x}$ and $\vec{y}$ body-fixed components

$$\begin{bmatrix} \dot{u} \\ \dot{v} \\ \dot{w} \end{bmatrix} = \mathbf{R}_I^b \begin{bmatrix} 0 \\ 0 \\ g \end{bmatrix} - \begin{bmatrix} 0 \\ 0 \\ \frac{T}{m} \end{bmatrix} - \begin{bmatrix} \frac{\mu}{m}u \\ \frac{\mu}{m}v \\ 0 \end{bmatrix}, \tag{6}$$

where μ is the drag force coefficient. The term μ can depend on several factors, but for nominal autonomous flight conditions it can be treated as a constant. We highlight that the changes required to implement the enhanced model are simply two terms added to the body-frame velocity equations. Reference [12] identifies this drag force as the rotor drag, although the detailed derivation somewhat obscures the simplicity and practicality of the model.

Using (6), the components of (2) can now be expressed as

$$\begin{bmatrix} \dot{\phi} \\ \dot{\theta} \\ \dot{\psi} \end{bmatrix} = \begin{bmatrix} 1 & \sin\phi\tan\theta & \cos\phi\tan\theta \\ 0 & \cos\phi & -\sin\phi \\ 0 & \frac{\sin\phi}{\cos\theta} & \frac{\cos\phi}{\cos\theta} \end{bmatrix} \begin{bmatrix} p \\ q \\ r \end{bmatrix}, \tag{7}$$

$$\begin{bmatrix} \dot{u} \\ \dot{v} \\ \dot{w} \end{bmatrix} = \begin{bmatrix} -g\sin\theta + (vr - wq) - \frac{F_{d_i}}{m} \\ g\sin\phi\cos\theta + (wp - ur) - \frac{\mu}{m}u \\ g\cos\phi\cos\theta + (uq - vp) - \frac{\mu}{m}v \end{bmatrix}. \tag{8}$$

The other terms in the $\dot{u}$ and $\dot{v}$ portions of (8) are due to gravity and the Coriolis acceleration. We discussed in the "Accelerometer Tutorial" why gravity is not measured by the accelerometers, and the Coriolis terms can be neglected for a quadrotor that depends on onboard sensors. We can therefore model the $\vec{x}$ and $\vec{y}$ accelerometer outputs a_{mi} and a_{mj} as directly

measuring the respective components of the drag force

$$h_1 \triangleq a_{mi} \approx -\frac{\mu}{m}u, \tag{9}$$

$$h_2 \triangleq a_{mj} \approx -\frac{\mu}{m}v. \tag{10}$$

Equations (9) and (10) are the two measurement functions included in (3).

Figure 4 illustrates the agreement between the actual accelerometer measurements and those predicted by equations (9) and (10). We generated Figure 4 using recorded time-stamped accelerometer and pose data during a manually controlled flight. The accelerometer measurements were from the onboard sensors and the pose measurements from a motion capture system. We used a filtered numerical derivative of the position measurements, expressed in the body-fixed frame of the quadrotor, for the u and v velocities in (9) and (10). The value for μ was determined using a least-squares fit of the data from several flights. We found that the error between the predicted and actual accelerometer measurements is modeled well as zero-mean and Gaussian.

Why Traditional Attitude Estimates Provide Some Benefit

Reference [21] offers some additional perspective on accelerometer measurements as they relate to the roll angle ϕ and the pitch angle θ on a quadrotor. Using (9) and (10) in (8) and ignoring the Coriolis forces, the time evolution of u and v from (8) can be written as

$$\begin{bmatrix} \dot{u} \\ \dot{v} \end{bmatrix} = \begin{bmatrix} -g\sin\theta - \frac{\mu}{m}u \\ g\sin\phi\cos\theta - \frac{\mu}{m}v \end{bmatrix}. \tag{11}$$

Consider for a moment just the first row of (11). Using a small angle approximation and

taking the Laplace transform gives the transfer function from θ to u as

$$u(s) = \frac{\frac{-gm}{\mu}}{\frac{m}{\mu}s + 1}\theta(s). \tag{12}$$

Substituting (9) in (12) we obtain

$$a_{mi}(s) = \frac{g}{\frac{m}{\mu}s + 1}\theta(s) \triangleq H(s)\theta(s). \tag{13}$$

By similar arguments, we find that

$$a_{mj}(s) = \frac{-g}{\frac{m}{\mu}s + 1}\phi(s) = -H(s)\phi(s). \tag{14}$$

Equations (13) and (14) describe the first-order response relating the changes in attitude to the accelerometer measurements, where $H(s)$ is a low-pass filter.

Figure 5 shows the true pitch angle for a quadrotor measured by a motion capture system, as compared to the traditional attitude estimate described in the "Accelerometer Tutorial" (sidebar) using actual accelerometer measurements. We have also superimposed the result of filtering the true pitch angle with $H(s)$ as given in (13). The traditional attitude estimate based on accelerometer measurements agrees well with the low-pass filtered pitch angle.

The traditional attitude method given in the "Accelerometer Tutorial" (sidebar) is based on the assumption of static equilibrium. The time constant m/μ governs how quickly the accelerometer measurements react to a step change in the roll or pitch angle. For a heavier quadrotor used for onboard vision experiments, $m = 2.75$ kg and $\mu \approx 0.77$. In this case it would take the accelerometer (and therefore the traditional attitude estimate) more than 10 seconds to reach 95% of its steady-state value. Even for the nimble Hummingbird quadrotor by Ascending Technologies, it takes approximately 3 seconds to approach steady state. Long

before the accelerometer-based attitude estimate becomes valid, the quadrotor will reach speeds that degrade onboard sensor data or that make collision in a cluttered environment likely.

It is well known that angle estimation using the traditional approach does not describe fast attitude changes, even if the reason behind it is less understood. To compensate, gyroscopes can be used to predict attitude over the short term. Accelerometers are then used to correct the estimates in a measurement update. However, without accounting for the fact that the accelerometers on the quadrotor measure scaled velocities, as shown in (9) and (10), the measurement update will drag the estimates toward the low-pass filtered attitude and not the true attitude. This estimation approach works reasonably well during flights with gradual attitude changes, but produces less accurate estimates than are possible.

Observer Design

In this section, we present several filter design options using the drag-force-enhanced model for the case where the states $\mathbf{x}_{imu} = [\phi, \theta, u, v]^\top$ will be estimated using only IMU data. This application is of interest when designing a filter for attitude estimation such as is typically available on quadrotor autopilots.

Linear Fixed-gain Filter

A simple approach to observer design is to make approximations so that the state propagation and measurement equations are linear. In this case, (2) and (3) are replaced by

$$\dot{\mathbf{x}}_{imu} = \mathbf{A}\mathbf{x}_{imu} + \mathbf{B}\mathbf{u},$$

$$\mathbf{y}_{acc} = \mathbf{C}_{acc}\mathbf{x}_{imu},$$

where $\mathbf{A}$ and $\mathbf{B}$ are the appropriate Jacobians of (7) and (8) and $\mathbf{C}_{acc}$ is the Jacobian of (9) and (10). We will assume Coriolis forces are negligible and evaluate the Jacobians at hover. We further simplify the design by choosing a fixed observer gain.

We take $\mathbf{y}_{acc} = [a_{mi}, a_{mj}]^\top$ as modeled by (9) and (10) as the only elements of (3). Using the inputs $\mathbf{u} = [p, q, r]^\top$ gives

$$\mathbf{A} = \begin{bmatrix} 0 & 0 & 0 & 0 \\ 0 & 0 & 0 & 0 \\ 0 & -g & \frac{\mu}{m} & 0 \\ g & 0 & 0 & \frac{\mu}{m} \end{bmatrix},$$

$$\mathbf{B} = \begin{bmatrix} 1 & 0 & 0 \\ 0 & 1 & 0 \\ 0 & 0 & 0 \\ 0 & 0 & 0 \end{bmatrix},$$

$$\mathbf{C}_{acc} = \begin{bmatrix} 0 & 0 & \frac{\mu}{m} & 0 \\ 0 & 0 & 0 & \frac{\mu}{m} \end{bmatrix}.$$

State estimates are propagated using

$$\dot{\mathbf{x}}_{imu} = \mathbf{A}\mathbf{x}_{imu} + \mathbf{B}\mathbf{u} + \mathbf{L}_{fg}(\mathbf{y} - \mathbf{C}_{acc}\mathbf{x}_{imu})$$

where the observer gain $\mathbf{L}_{fg}$ is chosen using the *lqr* function in Matlab. Because of its simplicity, this linear fixed-gain filter is the most practical choice for an embedded processor versus the extended Kalman filters presented below. Results using this filter will be presented later in the article.

EKF with Known μ

The Extended Kalman Filter (EKF) offers improved performance over the linear fixed-gain filter at the expense of increased complexity. Appropriate elements of the nonlinear equations (7) and (8) are used in a separate prediction step to propagate $\mathbf{x}_{imu}$ forward in time, and Jacobians $\mathbf{A}$, $\mathbf{B}$, and $\mathbf{C}_{acc}$ are constantly reevaluated using the current state estimate.

However, most of the increased complexity arises in maintaining the uncertainty of the state estimates, $\mathbf{P}$, and calculating the variable filter gain. The uncertainty is propagated using

$$\dot{\mathbf{P}} = \mathbf{AP} + \mathbf{PA}^\top + \mathbf{BR}_{gyro}\mathbf{B}^\top + \mathbf{Q}. \tag{15}$$

The process uncertainty in (15) is modeled in two parts. Matrix $\mathbf{Q}$ is a hand-tuned, diagonal matrix that we often use only to model the propagation of bias states. Since the inputs $\mathbf{u}$ are gyroscope measurements, and $\mathbf{B}$ is the matrix that specifies how the gyroscopes affect the state evolution, $\mathbf{R}_{gyro}$ is the covariance of the noise on those sensors. Since we can measure the noise characteristics of the gyroscopes, using the $\mathbf{BR}_{gyro}\mathbf{B}^\top$ term makes the filter easy to tune and more accurate than assuming a generic, diagonal process noise matrix for all of the states.

The accelerometer measurement update is given by

$$\mathbf{L} = \mathbf{P}^-\mathbf{C}_{acc}^\top \left(\mathbf{R}_{accel} + \mathbf{C}_{acc}\mathbf{P}^-\mathbf{C}_{acc}^\top\right)^{-1},$$

$$\mathbf{P}^+ = (\mathbf{I} - \mathbf{LC}_{acc})\mathbf{P}^-,$$

$$\mathbf{x}_{imu}^+ = \mathbf{x}_{imu}^- + \mathbf{L}\left(\mathbf{y}_{acc} - \mathbf{C}_{acc}\mathbf{x}_{imu}^-\right).$$

The notation Y^- and Y^+ indicates a variable Y before and after the measurement update. We use $\mathbf{R}_{accel}$ to denote the covariance of the accelerometer measurement, and $\mathbf{I}$ is an appropriate

identity matrix. Results for this filter will be given later in the article.

EKF with Estimated μ

The filters given in the previous two sections assume that the rotor drag coefficient μ is known. In this section we relax that assumption and add μ to the state vector of the EKF and estimate it simultaneously with the other states. In "Observability of μ" (sidebar) we show that μ is observable. In the remainder of the paper, we will designate the filter derived in this section as EKF-μ. We have found that μ can be estimated accurately in a filter using only IMU data. Over several datasets, the filter-estimated μ stays within about 5% of the truth value estimated using a motion capture system. When added to the estimated state the propagation of μ is modeled as a random walk.

Estimating μ as a state of the EKF provides substantial benefit over other approaches that use an improved dynamic model. In reference [12] the authors describe a hand tuning process accomplished by comparing several quantities from the vehicle and their counterparts given by a GPS-driven attitude heading reference system (AHRS). Since the AHRS cannot be collocated with the vehicle's IMU, the parameter μ must be tuned simultaneously with the position and attitude differences that make the accelerometers on the AHRS agree with those of the vehicle. Reference [1] relies on an expensive motion capture system to provide flight data that they compare to control commands; a system identification process is then used to determine the right values for a damping coefficient similar in nature to μ.

Because EKF-μ estimates an additional state, its performance suffers as compared to the filters that use a predetermined value for μ. Figure 6 illustrates this by comparing the root-

mean-squared (RMS) error in body frame velocity over several initial values of μ. As would be expected, EKF-μ is robust to poor initial estimates of μ. If μ cannot be determined beforehand, we suggest EKF-μ be used in an initial manual flight to produce an estimate. In subsequent flights, with perhaps some minor hand tuning of μ, one of the other filters should be used to avoid a decrease in estimation accuracy. Figure 6 shows that there is a reasonable range of values for the estimate of μ that enable the Fixed-Gain and EKF filters to perform well.

IMU-Only Results

We use a MikroKopter [22] quadrotor dipicted in Figure 2 and a motion capture system, in Figure 3, from Motion Analysis [23] to generate the data used in these results. The quadrotor provides accelerometer and gyroscope measurements at 40 Hz. We use this low rate, much lower than is typically used, to highlight the benefits of using the drag-force-enhanced model. We receive pose information for the quadrotor from the motion capture system at 200 Hz. A filtered numerical derivative of the position information is used to estimate the true velocity. All the data was first recorded from a 250 second manually-controlled flight and then processed offline so that comparisons between different filters would be valid.

Comparison Filters

As a baseline to compare against, we present results from two filters that rely on the traditional attitude approach. The first is a fixed-gain linear filter described by

$$\dot{\mathbf{x}}_n = \begin{bmatrix} p \\ \\ q \end{bmatrix} + \mathbf{L}_n \left(\mathbf{x}_{accel} - \mathbf{x}_n \right),$$

where $\mathbf{x}_n = [\phi, \theta]^\top$. The fixed observer gain $\mathbf{L}_n$ is selected to prevent the estimates from drifting while still tracking fast changes as best as possible. We tuned $\mathbf{L}_n$ to produce results qualitatively similar to those from a popular commercial quadrotor. The vector $\mathbf{x}_{accel}$ is an estimate of ϕ and θ based on the traditional attitude method (S4) and (S5). We designate this filter the *Traditional FG* filter.

The second filter is the explicit nonlinear complementary filter developed in [24]. This filter estimates the rotation matrix $\hat{\mathbf{R}}$ between the body-fixed reference frame and the inertial reference frame, as well as the biases on the gyroscopes $\hat{\mathbf{b}}$. The filter is implemented using

$$\begin{aligned}
\dot{\hat{\mathbf{R}}} &= \hat{\mathbf{R}}\left(\left(\mathbf{u} - \hat{\mathbf{b}}\right)_\times + k_P\left(\omega_{mes}\right)_\times\right), \quad \hat{\mathbf{R}}(0) = \hat{\mathbf{R}}_0 \\
\dot{\hat{\mathbf{b}}} &= -k_I \omega_{mes} \\
\omega_{mes} &= \sum_{i=1}^{n} k_i v_i \times \hat{v}_i, \quad k_i > 0,
\end{aligned}$$

where the notation $()_\times$ refers to the matrix form of the cross product, and v_i are vectorial measurements. Using only IMU information without a magnetometer, there is only one vectorial measurement: the gravity measurement discussed in the "Accelerometer Tutorial". The implementation completed for this paper was iteratively hand-tuned to provide the minimum RMS error in attitude for the dataset considered. The gains were $k_P = 0.5$ and $k_I = 0.05$ for the results presented below. We designate this as the *Complementary* filter.

Attitude Results

Figure 7 plots the error in the estimates for a small portion of the manual flight; results for the pitch angle θ are similar. The figure compares the performance of the *Traditional FG* and

Complementary filters with the drag-force-enhanced, linear fixed-gain filter we have described in this article.

The filters' performance is further described by Table I which presents the RMS error results for all of the filters over the entire flight. Notice in Table I that the other filters we have designed using the enhanced model offer improved performance over the linear fixed-gain filter, but at increased computational cost. We chose to represent the results of the linear fixed-gain filter in Figure 7 as it is more relevant in an IMU-only, embedded scenario.

Velocity Results

In addition to improving attitude estimates, the enhanced model also provides information on the body-frame velocities u and v that would be otherwise unavailable using only IMU measurements. Table II documents the RMS errors for velocity estimates using the drag-force-enhanced model in the filters presented above. Figure 8 illustrates estimates of u produced using the linear fixed-gain filter and the EKF. Note that velocity estimates for the *Traditional FG* and *Complementary* filters are absent from these results as these filters do not provide velocity estimates.

Although the performance does not appear outstanding in Table II and Figure 8, we note that these results are produced using only inexpensive MEMS accelerometers and gyroscopes at low data rates. The fact that the improved model offers information on velocity along with high-quality attitude estimates is an additional advantage of the proposed approach. The velocity estimates from the drag-force-enhanced model reduce the need for fast position updates that traditional approaches require [20].

Results During Aggressive Maneuvers

We have also found that estimation using the drag-forced enhanced model is robust to aggressive maneuvers despite the near-hover assumption made in [12] to derive the model. Figure 9 shows estimates of θ for a segment of aggressive flight. The quadrotor experiences pitch angles in excess of 45 degrees that are estimated well by the method we propose.

The performance improvements shown here are due to the more correct model of the physical system that accounts for the rotor drag. The gyroscope measurements provide information for the fast changes in angle and the accelerometer corrections accurately constrain the drift. In the traditional approach, if the gyroscope measurements are trusted too much in order to track fast angular changes, the attitude estimates drift rapidly. To constrain the drift, the accelerometer measurements must be weighted sufficiently, but using the wrong dynamic model results in inferior performance.

It is important to note that the filter tuning parameters were not modified for this flight segment, which highlights the robustness of the proposed estimators. The *Traditional FG* and *Complementary* filters could be tuned for better performance during aggressive maneuvers but then performance near hover would suffer. As an alternative, an adaptive control or gain scheduling approach could be implemented on those filters to provide improved estimates for a broader flight regime, but at the expense of increased complexity.

Position Dead-reckoning Results

In this section we illustrate the significant results that are possible due to the improved accuracy given by the drag-force-enhanced model. We completed an experiment where the IMU information from the quadrotor was used to dead reckon the global position. We implemented this experiment with two filters: the Traditional EKF and the Drag-Force EKF.

The Traditional EKF is a combination of the two methods presented in the "Accelerometer Tutorial". The *Traditional FG* filter, explained above, provides the attitude estimates using the accelerometer and gyroscope measurements according to the traditional attitude method. Then the filter estimates the global position by integrating accelerometer measurements using the integrated velocity method.

The Drag-Force EKF is an augmented version of the EKF with Known μ method, which was derived above. The filter uses the gyroscopes and accelerometer measurement updates (9) and (10) to estimate the attitude and velocity. We augmented this filter to also include north and east position states, which are estimated by integrating the velocity estimates.

In both filters the standard kinematic relationship between velocity and position is used to estimate the position using velocity estimates. Initialization of the position estimates at the starting global location is the only input position information provided to either filter during the whole flight.

Figure 10 shows north and east position dead-reckoning estimates obtained using only the IMU information available during the first ten seconds of the quadrotor flight. Note how the Drag-Force EKF estimates trend well with the global position while the estimates from the

Traditional EKF do not. Figure 11 plots the norm of the north and east error for the Traditional EKF and the Drag-Force EKF. Note the vast difference in drift rate between the two approaches over the whole flight.

The point of these results is to demonstrate how much information the IMU can provide to the quadrotor state estimates when a valid model is employed. The basic position information provided by this approach can contribute to a lower dependence on exteroceptive sensor or GPS information [20]. Correctly modeling the accelerometer measurements has a significant impact on position, velocity, and attitude estimates.

Conclusion

We have shown that assumptions behind the attitude method for measuring the gravity vector are flawed when applied to a quadrotor, even though the approach provides some benefit. When designing an estimator for a quadrotor it is too restrictive to assume static equilibrium. The forces acting on the quadrotor will only sum to zero at hover or after a long period of time at a fixed attitude.

Using only IMU data, the EKF and the linear fixed-gain filter based on the drag-force-enhanced model provide a trade-off between complexity and performance. Each provides an improvement in attitude estimates compared to typical approaches, even during aggressive maneuvers, while also providing significant information about velocity. The velocity estimates, in turn, can be used effectively by the EKF to provide position estimates based on dead reckoning that diverge relatively slowly. If μ is unknown, we have shown that it can be effectively estimated by including it in the state during accelerated flight. The accuracy of the estimates we provided

from the IMU-only filters could be further improved by increasing the data rate of the IMU.

We attribute the improvements shown in this article to the correct characterization of accelerometer measurement. This is a noteworthy advantage as IMU measurements are typically available at high rates and are comparatively inexpensive to process.

Acknowledgment

This research is supported through the U.S. Department of Defense SMART Scholarship program: `smart.asee.org`.

References

[1] A. Bachrach, S. Prentice, R. He, and N. Roy, "RANGE - Robust Autonomous Navigation in GPS-denied Environments," *Journal of Field Robotics*, vol. 28, no. 5, pp. 644–666, Sep. 2011.

[2] S. Shen, N. Michael, and V. Kumar, "Autonomous Multi-Floor Indoor Navigation with a Computationally Constrained MAV," in *IEEE Intl. Conf. on Robotics and Automation*, May 2011, pp. 20–25.

[3] L. Meier, P. Tanskanen, F. Fraundorfer, and M. Pollefeys, "PIXHAWK : A System for Autonomous Flight using Onboard Computer Vision," in *IEEE Int. Conf. on Robotics and Automation*, 2011, pp. 2992–2997.

[4] J. P. How, B. Bethke, A. Frank, D. Dale, and J. Vian, "Real-Time Indoor Autonomous Vehicle Test Environment," *IEEE Control Systems Magazine*, pp. 51–64, Apr. 2008.

[5] V. Kumar and N. Michael, "Opportunities and Challenges with Autonomous Micro Aerial Vehicles," in *15th International Sympossium on Robotics Research*, 2011.

[6] M. Hehn and R. D. Andrea, "Quadrocopter Trajectory Generation and Control," in *International Federation of Automatic Control World Congress*, 2011.

[7] G. Chowdhary, D. M. Sobers, C. Pravitra, A. Wu, C. Christman, H. Hashimoto, C. Ong, R. Kalghatgi, and E. N. Johnson, "Integrated Guidance Navigation and Control for a Fully Autonomous Indoor UAS," in *AIAA Guidance, Navigation and Control Conference Proceedings*, 2011.

[8] L. R. García Carrillo, A. E. Dzul López, R. Lozano, and C. Pégard, "Combining Stereo Vision and Inertial Navigation System for a Quad-Rotor UAV," *Journal of Intelligent &*

Robotic Systems, pp. 373–387, Aug. 2011.

[9] N. Guenard, T. Hamel, and R. Mahony, "A Practical Visual Servo Control for an Unmanned Aerial Vehicle," *IEEE Transactions on Robotics*, vol. 24, no. 2, pp. 331–340, Apr. 2008. [Online]. Available: ieeexplore.ieee.org/lpdocs/epic03/wrapper.htm?arnumber=4481181

[10] M. Blosch, S. Weiss, D. Scaramuzza, and R. Seigwart, "Vision Based MAV Navigation in Unknown and Unstructured Environments," in *IEEE Intl. Conf. on Robotics and Automation*, 2010, pp. 21–28.

[11] I. Sa and P. Corke, "System Identification, Estimation and Control for a Cost Effective Open-Source Quadcopter," in *IEEE Int. Conf. on Robotics and Automation*, 2012, pp. 2202–2209.

[12] P. Martin and E. Salaun, "The True Role of Accelerometer Feedback in Quadrotor Control," *IEEE Intl. Conf. on Robotics and Automation*, pp. 1623–1629, 2010.

[13] T. Madani and A. Benallegue, "Backstepping Control for a Quadrotor Helicopter," *IEEE/RSJ Intl. Conf. on Intelligent Robots and Systems*, pp. 3255–3260, Oct. 2006.

[14] R. Xu and U. Ozguner, "Sliding Mode Control of a Quadrotor Helicopter," *IEEE Conf. on Decision and Control*, pp. 4957–4962, 2006.

[15] T. Madani and A. Benallegue, "Control of a Quadrotor Mini-Helicopter via Full State Backstepping Technique," *IEEE Conf. on Decision and Control*, pp. 1515–1520, 2006.

[16] S. Bouabdallah, "Design and Control of Quadrotors with Application to Autonomous Flying," PhD, École Polytechnique Fédérale de Lausanne, 2007.

[17] A. A. Mian and W. Daobo, "Nonlinear Flight Control Strategy for an Underactuated Quadrotor Aerial Robot," in *IEEE Intl. Conf. on Networking, Sensing and Control*, 2008, pp. 938–942.

[18] S. Grzonka, G. Grisetti, and W. Burgard, "Towards a Navigation System for Autonomous

Indoor Flying," in *IEEE Intl. Conf. on Robotics and Automation*, no. Section III. Ieee, May 2009, pp. 2878–2883.

[19] R. Leishman, J. Macdonald, S. Quebe, J. Ferrin, R. Beard, and T. Mclain, "Utilizing an Improved Rotorcraft Dynamic Model in State Estimation," in *IEEE/RSJ Intl. Conf. on Intelligent Robots and Systems*, 2011.

[20] J. Macdonald, R. Leishman, R. Beard, and T. McLain, "Analysis of an Improved IMU-Based Observer for Multirotor Helicopters," *Journal of Intelligent & Robotic Systems (in review; preprint available from the authors)*.

[21] C. Chamberlain, "System Identification, State Estimation, and Control of Unmanned Aerial Robots," Master's Thesis, Brigham Young University, Provo, UT, Apr. 2011.

[22] "Mikrokopter." [Online]. Available: www.mikrokopter.de/ucwiki/en/MikroKopter

[23] "Motion Analysis Corp." [Online]. Available: www.motionanalysis.com/

[24] R. Mahony, T. Hamel, and J.-M. Pflimlin, "Nonlinear Complementary Filters on the Special Orthogonal Group," *IEEE Transactions on Automatic Control*, vol. 53, no. 5, pp. 1203–1218, 2008.

[25] M. Vidyasagar, *Nonlinear Systems Analysis*. Prentice-Hall, 1993.

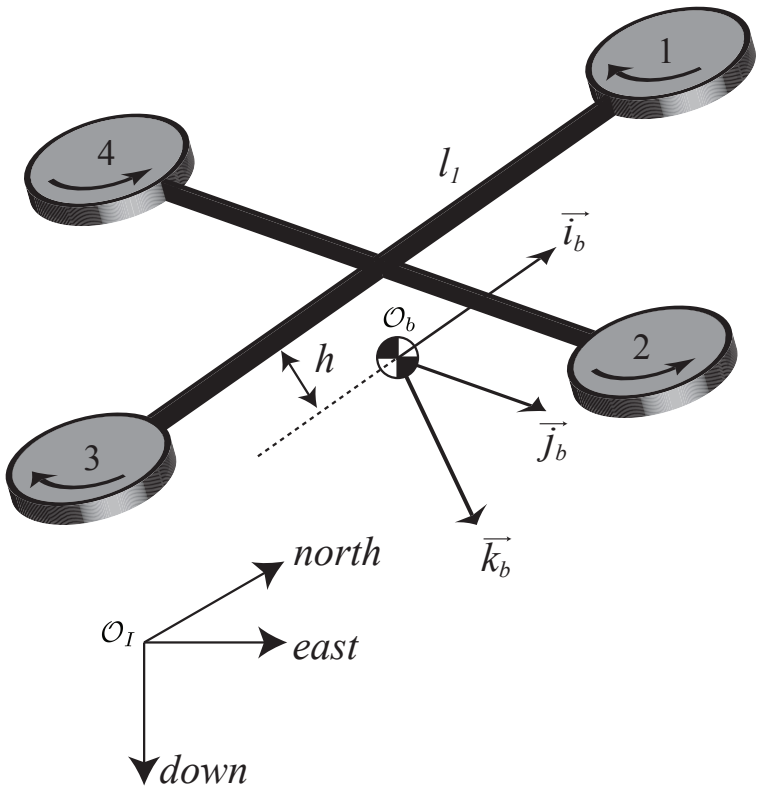

Figure 1. Schematic of a Quadrotor. A schematic representation of the quadrotor showing coordinate frames and notation used in the article. The inertial coordinate frame has its arbitrary origin at $\mathcal{O}_I$ with right-handed axes oriented in north, east, and down (i.e. aligned with gravity) directions. The body-fixed reference frame has its origin, $\mathcal{O}_b$, at the quadrotor's center of mass, assumed here to be some distance h directly below the quadrotor's geometric center. The body frame $\vec{i}_b$ and $\vec{j}_b$ axes are parallel with the vectors from the geometric center to motors 1 and 2. The $\vec{k}_b$ axis is oriented to complete a right-handed coordinate system. The motors rotate in the directions shown.

Figure 2. Hovering Quadrotor. A quadrotor from MikroKopter that was used in the experiments. The vehicle is hovering using the measurements from the motion capture system. ©Jaren Wilkey, BYU Photo

Figure 3. Motion Capture Environment. Here is the motion capture environment where all the testing was conducted for this research. We use a motion capture system from Motion Analysis. The system provides 6DoF pose information at 200 Hz with sub-degree and sub-millimeter accuracy.

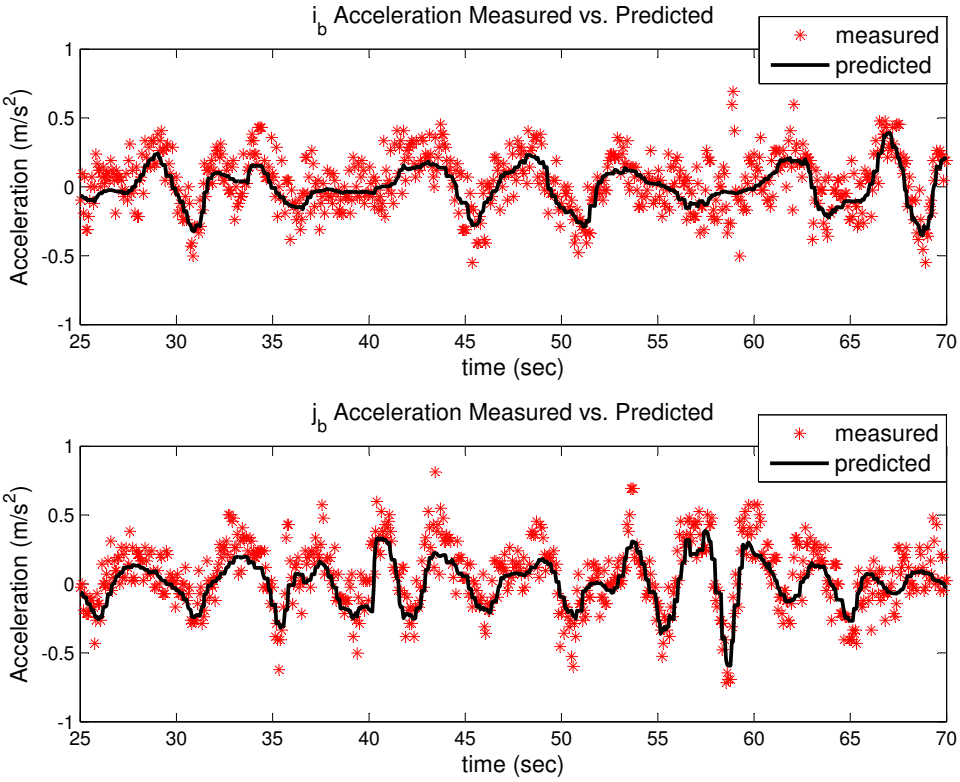

Figure 4. Predicted and Actual Accelerometer Measurements. The actual accelerometer measurements for a nominal indoor flight are plotted against those predicted by (9) and (10). We generated this figure using time-stamped accelerometer and pose data recorded during a manually-controlled flight.

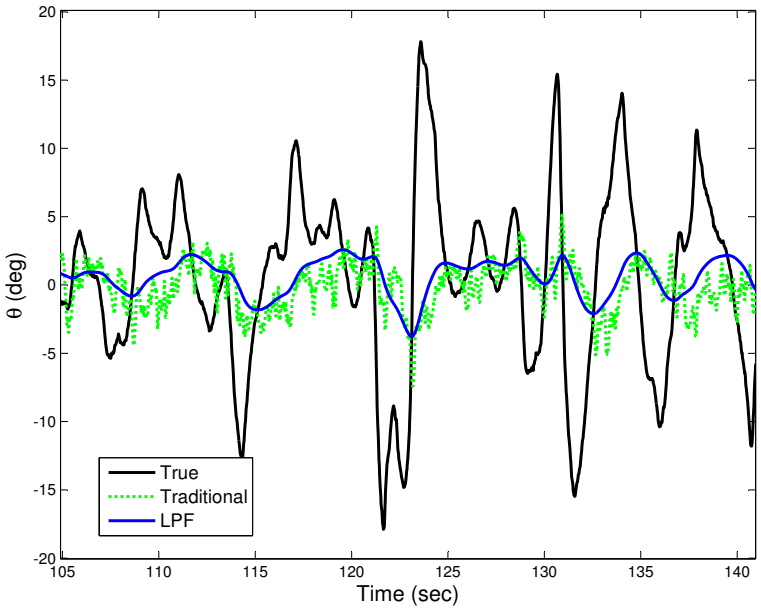

Figure 5. Pitch Angle Comparison. Comparison of the true pitch angle θ, the traditional attitude approximation, and a low-pass filtered θ for a small portion of a flight. Notice how closely the traditional attitude estimation method results approach those of the low-pass filtered pitch angle.

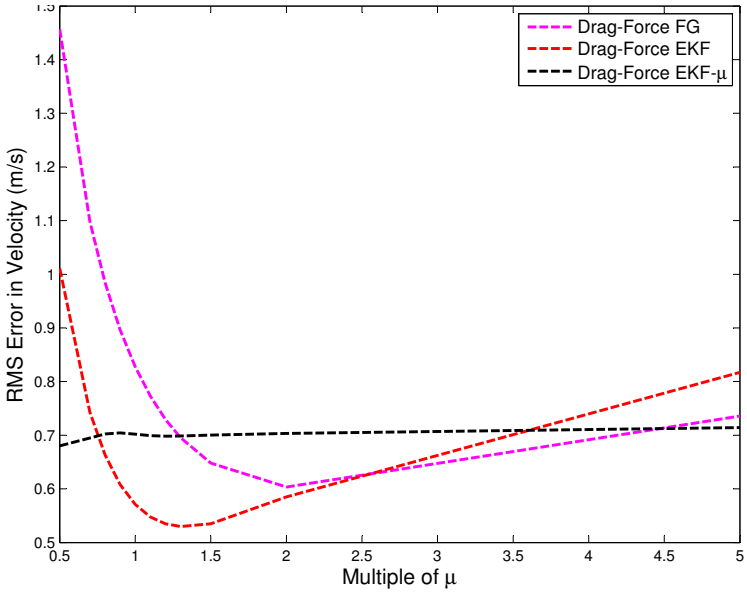

Figure 6. RMS Error in Velocity. RMS errors in velocity for the various filters when the initial estimate of μ is a multiple of the true value. The Fixed Gain filter and EKF use the initial, but incorrect, value of μ throughout the entire flight. With EKF-μ, the value evolves in time. It is interesting to note that the Fixed Gain and EKF still provide low RMS values over a wide range of incorrect estimates of μ.

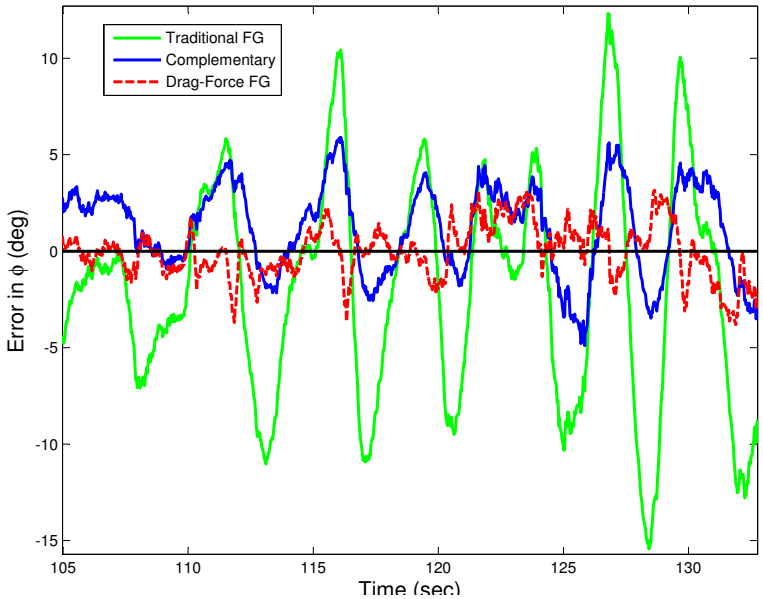

Figure 7. Error in ϕ Estimates. The error in the roll angle ϕ over a small window of the manual flight for the Traditional FG, Complementary and drag-force enhanced fixed gain filters. Since the plot is of error, smaller values denote increased performance.

TABLE I

RMS ERROR FOR ϕ AND θ. THE COMBINED RMS ERRORS FROM THE VARIOUS FILTERS FOR ϕ AND θ FROM A MANUAL FLIGHT.

RMS Error for Attitude Estimates	
Filter	**RMS of ϕ and θ (deg)**
Traditional FG	7.27
Complementary	5.66
Drag-Force Linear Fixed-Gain	2.80
Drag-Force EKF	2.16
Drag-Force EKF-μ	2.23

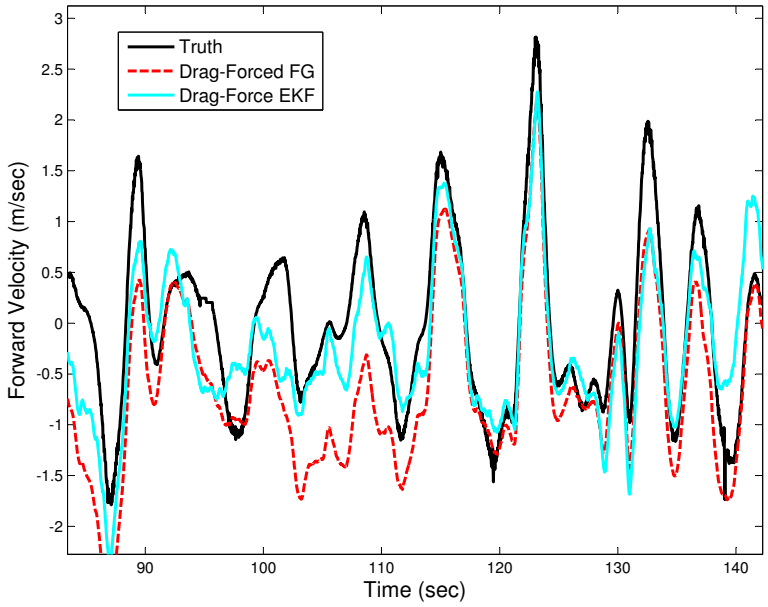

Figure 8. IMU-Only Velocity Results. Body-frame velocity u truth versus the drag-force fixed-gain filter and EKF estimates for a small portion of a flight. Velocity estimates are not available when using only IMU data with the traditional approaches. Only IMU information is used to produce these estimates. Only the drag-force enhanced filter estimates are shown;

TABLE II

RMS ERROR ON VELOCITY. THE COMBINED RMS ERRORS FOR THE VELOCITY ESTIMATES u AND v USING THE DRAG-FORCE ENHANCED MODEL.

RMS Errors for Velocity Estimates	
Filter	**RMS of u and v (m/s)**
Traditional FG	N/A
Complementary	N/A
Drag-Force Fixed-Gain	0.87
Drag-Force EKF	0.60
Drag-Force EKF-μ	0.67

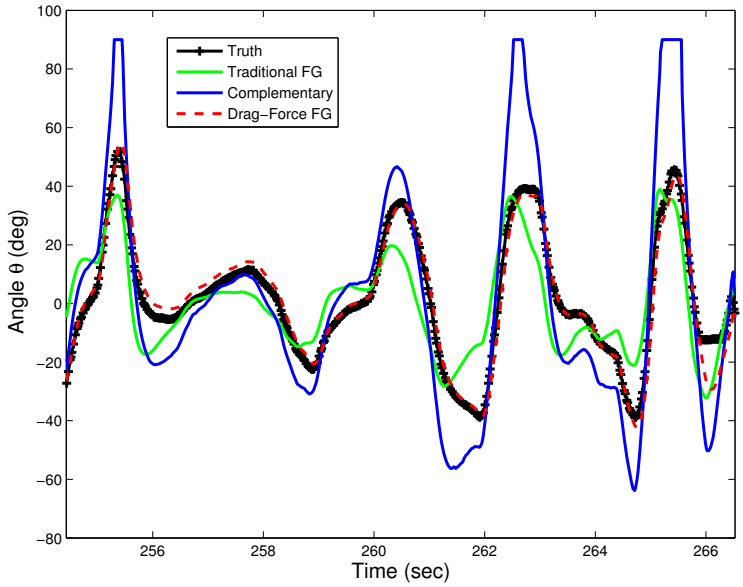

Figure 9. Pitch Angle During Aggressive Flight. This figure plots the true pitch angle θ and its estimates using the Traditional FG, Complementary, and drag-force-enhanced fixed-gain estimators during an aggressive flight. Notice that the linear fixed-gain filter for the enhanced model provides accurate estimates despite the large angles that are experienced. The filter parameters are identical to those used to produce the previous plots.

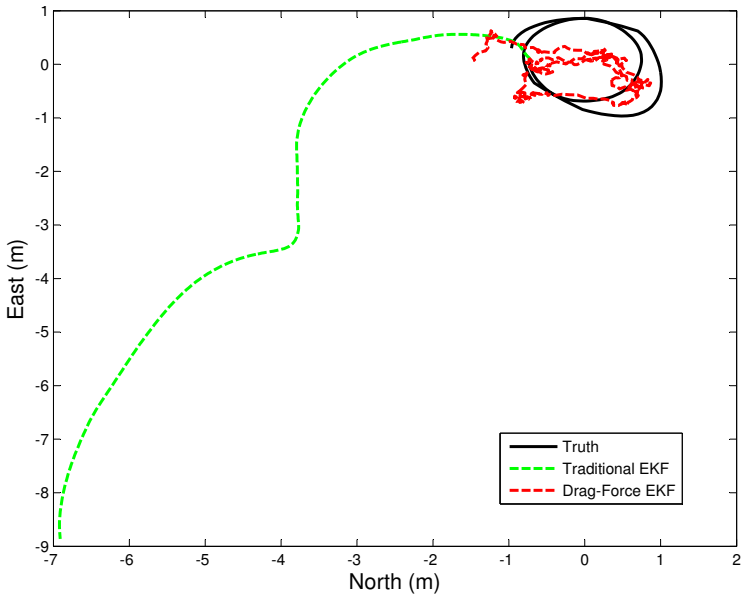

Figure 10. Position Dead-reckoning Results. These position results were obtained using only the IMU information available from the first 10 seconds of a manual quadrotor flight. The Traditional EKF uses the integrated velocity method mentioned in the"Accelerometer Tutorial" by integrating accelerometer values to obtain position estimates. The Drag-Force EKF uses the drag-force-enhanced model accelerometer measurement updates to estimate velocity and then integrates the velocity estimates to estimate position. Position information was used to initialize the estimates to the starting global position. Note how the improved EKF estimates trend with the global position while the estimates from the traditional approach walk off the chart. This demonstrates the importance of IMU information to the quadrotor state estimates when a valid model is employed.

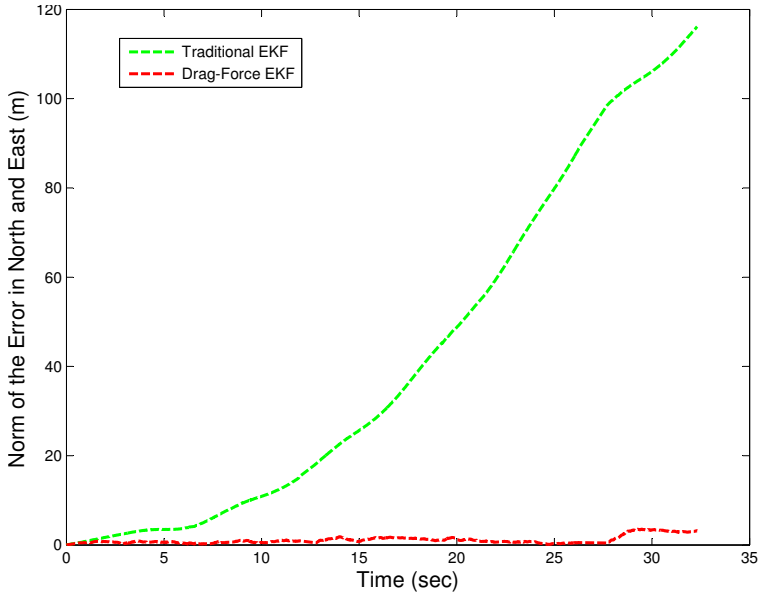

Figure 11. Norm of North and East Position Error. The norm of the north and east dead-reckoning position error for the Traditonal EKF and the Drag-Force EKF is shown. IMU measurements are the only sensor information provided to the two filters. Note the differences in the drift rate between the two approaches. Using the Drag-Force EKF will allow less-frequent exteroceptive and/or GPS updates because of the much lower drift rate using only the IMU information.

Sidebar 1: Accelerometer Tutorial

If $\mathbf{a} \in \mathbb{R}^3$ represents the acceleration of a vehicle, m is the mass, and $\mathbf{F}_T \in \mathbb{R}^3$ is the total external force acting on the vehicle, then Newton's second law states that

$$\mathbf{a} = \frac{1}{m}\mathbf{F}_T. \tag{S1}$$

However, accelerometers do not measure the total acceleration $\mathbf{a}$. Accelerometers measure the specific acceleration, meaning the difference between the acceleration of the vehicle and gravitational acceleration.

Figure S1 shows a simplified diagram of a one-axis accelerometer, where a proof-mass is attached by a flexure to the housing of the accelerometer. When the proof mass undergoes an acceleration that is different than the acceleration experienced by the housing, the proof mass deflects and a non-zero measurement is produced. With the accelerometer in Figure S1 on a horizontal surface, the normal force offsets the force due to the weight. The proof-mass, which does not experience the normal force, deflects under the influence of gravity, causing the accelerometer to measure an upward acceleration of 1 g. On the other hand, during free fall, gravity would accelerate both the housing and the proof-mass, resulting in a measurement of zero.

The output of a three-axis accelerometer mounted on a rigid body is then given by

$$\mathbf{a}_m = \frac{1}{m}\left(\mathbf{F}_T - \mathbf{F}_g\right), \tag{S2}$$

where $\mathbf{a}_m \in \mathbb{R}^3$ is the measured acceleration and $\mathbf{F}_g \in \mathbb{R}^3$ is the force due to gravity. Equation (S2) states that for an accelerometer to measure the effect of gravity only, all the external forces must sum to zero.

Throughout the article we assume that the axes of the accelerometer are aligned with the body-frame axes. We also assume that the accelerometer has been properly calibrated to remove misalignment errors and cross-axis sensitivity.

Below we detail two different methods for state estimation using accelerometers. Many researchers have shown that using one of these methods to fuse accelerometers with an exteroceptive sensor increases performance compared to using the exteroceptive sensor alone.

Accelerometer-based Attitude Estimation

From (S2), when the sum of external forces is zero the accelerometers will measure

$$\mathbf{a}_m = -\frac{1}{m}\mathbf{F}_g. \tag{S3}$$

Let $\mathbf{a}_m^b \triangleq (a_{mi}, a_{mj}, a_{mk})^\top$, represent the acceleration measured in the body-frame axes. In the inertial frame the force of gravity is $\mathbf{F}_g = (0, 0, mg)^\top$. Expressing (S3) in the body frame gives

$$\begin{aligned}\begin{bmatrix} a_{mi} \\ a_{mj} \\ a_{mk} \end{bmatrix} &= \mathbf{R}_I^b \begin{bmatrix} 0 \\ 0 \\ -g \end{bmatrix}, \\ &= \begin{bmatrix} g\sin\theta \\ -g\sin\phi\cos\theta \\ -g\cos\phi\cos\theta \end{bmatrix},\end{aligned}$$

where ϕ is the roll angle and θ is the pitch angle of the ground vehicle. The roll and pitch angles can therefore be estimated as

$$\hat{\phi}_{\text{accel}} = \tan^{-1}\left(\frac{a_{mj}}{a_{mk}}\right) \tag{S4}$$

$$\hat{\theta}_{\text{accel}} = \sin^{-1}\left(\frac{a_{mi}}{g}\right). \tag{S5}$$

This estimation method, expressed by (S4) and (S5), will be termed the traditional attitude method. We note here that the underlying assumption required for this method of zero external forces is rarely met during quadrotor flight.

Accelerometer-Based Velocity Estimation

If the attitude is known, measured accelerations can be integrated to estimate velocity using

$$\dot{\mathbf{v}}^b = \mathbf{a}_m^b + \frac{1}{m}\mathbf{R}_I^b\mathbf{F}_g. \tag{S6}$$

where $\mathbf{v}^b = (u, v, w)^\top$ is the velocity expressed in the body-fixed frame. It is critical to note here that this method of using accelerometers is sensitive to the underlying assumption of known attitude. The traditional attitude method should not be used to provide the necessary attitude estimates since it requires that $\dot{\mathbf{v}}^b = 0$. In the remainder of this article we will refer to this approach as the integrated velocity method.

Accelerometers on Quadrotors

Quadrotors obviously differ from ground vehicles because of the thrust required to keep them airborne. Yet many researchers using quadrotors treat them as ground vehicles with respect to accelerometer measurements. Quite often a variant of the traditional attitude method provides IMU-based estimates of attitude to a higher-level observer. This second observer then uses the integrated velocity method despite the fact that the methods' assumptions are contradictory.

As a simple example, when a quadrotor rests on an inclined surface, as shown in the left half of Figure S2, it experiences a normal force $\mathbf{F}_n$, a friction force $\mathbf{F}_f$ and the force due to gravity $\mathbf{F}_g$. The summation of forces in the body frame is

$$\mathbf{F}_T = \mathbf{R}_I^b \mathbf{F}_g - \mathbf{F}_n - \mathbf{F}_f.$$

Consequently the accelerometer measures

$$\mathbf{a}_m^b = \frac{1}{m}(\mathbf{F}_T - \mathbf{R}_I^b \mathbf{F}_g) = \frac{1}{m}\begin{bmatrix} -F_f \\ 0 \\ -F_n \end{bmatrix},$$

and (S5) can be used to correctly find the pitch angle.

When the quadrotor is in the air with a similar attitude, the forces are usually assumed to be $\mathbf{F}_g$ and the thrust $\mathbf{F}_t$; all other forces are assumed negligible. The thrust force $\mathbf{F}_t$ and moment $\mathbf{M}_t$ are resolved from the individual thrust forces acting at each propeller. This would give the total force, in the body-fixed reference frame, as

$$\mathbf{F}_T \approx -\mathbf{F}_t + \mathbf{R}_I^b \mathbf{F}_g.$$

According to the model, the accelerometers would then measure

$$\mathbf{a}_m^b = \frac{1}{m}(\mathbf{F}_T - \mathbf{R}_I^b \mathbf{F}_g) = \frac{1}{m}\begin{bmatrix} 0 \\ 0 \\ -F_t \end{bmatrix}.$$

Clearly in this situation the attitude cannot be determined using (S4) and (S5) since, according to the model, the body frame $\vec{i}$ and $\vec{j}$ accelerometers should always measure zero. It would also be invalid to integrate these values to find the vehicle velocities. Still, many researchers make productive use of the traditional attitude and velocity methods within control and estimation schemes. The discrepancy is explained by nontrivial forces that are missing in the model.

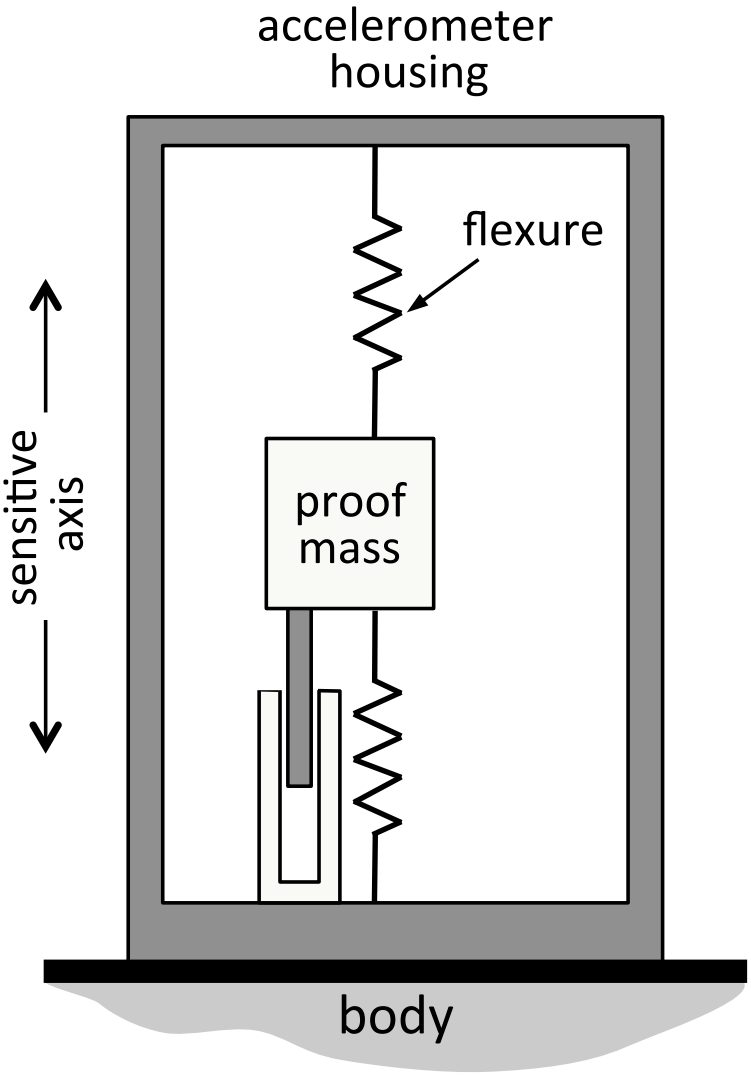

Figure S1. Simplified diagram of an accelerometer. When the proof mass undergoes an acceleration that is different than the acceleration experienced by the housing, the proof mass deflects and a non-zero measurement is produced.

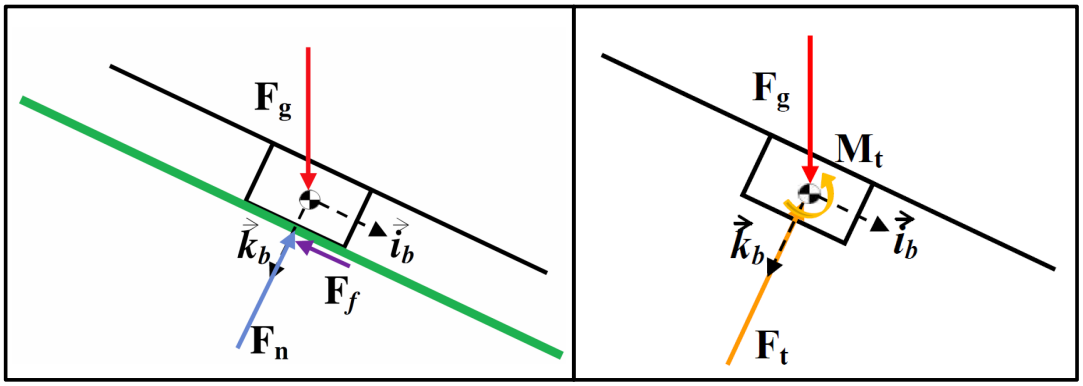

Figure S2. Quadrotor Free-body Diagrams. Free-body diagrams of a quadrotor in two scenarios. The left image shows the forces when the quadrotor is sitting on an inclined surface. The right image illustrates the forces according to the standard model when the quadrotor is at a constant attitude in the air and M_t is zero.

Sidebar 2: Observability of μ

In this section we demonstrate the observability of the drag coefficient μ when it is included in the state. We note that observability is a necessary condition for filter convergence. As a review, we briefly present the theory of nonlinear observability. Afterwards we provide the conditions where the longitudinal quadrotor system is locally observable with μ included in the vehicle state. This overview is based on a more detailed presentation of the theory in [25].

Theory

Let $\mathbf{x} \in X$, where X is an open subset of $\mathbb{R}^N$, represent the state of the nonlinear system

$$\dot{\mathbf{x}} = \mathbf{f}(\mathbf{x}) + \sum_{i=1}^{m} \mathbf{g}_i(\mathbf{x}) u_i, \tag{S1}$$

with n nonlinear outputs of the form

$$y_j = h_j(\mathbf{x}), \;\; j = 1...n, \tag{S2}$$

which form the vector output function $\mathbf{y}(y_1(\mathbf{x}), ..., y_n(\mathbf{x}), \mathbf{u})$. Further, let $S(X)$ and $V(X)$ respectively designate the set of all scalar-valued smooth functions and the set of all vector fields (i.e. column vectors on smooth functions) on X. The functions $\mathbf{f}(\mathbf{x})$, $\mathbf{g}_i(\mathbf{x}) \in V(X)$ are the nonlinear functions of the state and the m time-varying scalars u_i are the (known) inputs that drive the system.

Given (S1) and (S2), we can say that two states $\mathbf{x}_0$ and $\mathbf{x}_1$ are **distinguishable** if there exists an input function $\mathbf{u}(\cdot)$ such that

$$\mathbf{y}(y_1(\mathbf{x}_0), ..., y_n(\mathbf{x}_0), \mathbf{u}) \neq \mathbf{y}(y_1(\mathbf{x}_1), ..., y_n(\mathbf{x}_1), \mathbf{u}). \tag{S3}$$

The system is said to be **locally observable** at a point $\mathbf{x}_0 \in X$ if there exists a neighborhood $\mathcal{N}(\mathbf{x}_0)$ around $\mathbf{x}_0$ such that every $\mathbf{x} \in \mathcal{N}(\mathbf{x}_0)$, other than $\mathbf{x}_0$, is distinguishable from $\mathbf{x}_0$. We can say that the system is **locally observable** if it is locally observable at each point $\mathbf{x}_0 \in X$.

It can be shown that a system is locally observable at a point $\mathbf{x}_0 \in X$ if there are a sufficient number of linearly independent vectors in the gradients of the measurement equations or the gradients of the Lie derivatives evaluated at $\mathbf{x}_0$. Recall that the Lie derivative of a function $\kappa \in S(X)$ with respect to some vector field $\omega \in V(X)$ is defined by the mapping

$$L_\omega \kappa \triangleq \frac{\partial \kappa(\mathbf{x})}{\partial \mathbf{x}} \cdot \omega(\mathbf{x}) : X \to \mathbb{R}.$$

Quadrotor Longitudinal States With μ

We will now analyze the observability of the longitudinal quadrotor system with μ included in the state. The longitudinal states of a quadrotor are $\mathbf{x} = [\theta, u, \mu]^\top$. Recall that θ is the pitch angle, u is the body-fixed forward velocity, and μ is drag coefficient. The longitudinal system is

$$\begin{bmatrix} \dot{\theta} \\ \dot{u} \\ \dot{\mu} \end{bmatrix} = \mathbf{f}(\mathbf{x}) + u_1 \mathbf{g}_1(\mathbf{x}) = \begin{bmatrix} 0 \\ -g\sin(\theta) - \frac{\mu}{m} u \\ \varsigma_\mu \end{bmatrix} + u_1 \begin{bmatrix} 1 \\ 0 \\ 0 \end{bmatrix}, \tag{S4}$$

where we assume that $\dot{\theta} = q$, the rotation rate about the body $\hat{j}$ axis. The acceleration due to gravity is g and m is the mass of the vehicle. The time propagation of μ is modeled as a random walk where ς_μ is a zero-mean, Gaussian random variable. The gyroscope measurement $u_1 = q$ is the input to the system.

The output of the system is the accelerometer measurement in the body $\hat{i}$ direction,

modeled as

$$y_1 = h_1(\mathbf{x}) = -\frac{\mu}{m}u. \tag{S5}$$

To show that the longitudinal system is locally observable at a point $\mathbf{x}_0 \in X$, we must find three vectors of the observability Grammian that are linearly independent at $\mathbf{x}_0$. We begin with finding the gradient of the output (S5)

$$\mathbf{d}h_1 = \begin{bmatrix} 0 & -\frac{\mu}{m} & -\frac{u}{m} \end{bmatrix}. \tag{S6}$$

Next we look among the first-order Lie derivatives. Due to the simplicity of $\mathbf{g}_1(\mathbf{x})$ in (S4), $\mathbf{d}L_{g1}h_1 = [0\ 0\ 0]$. We then consider

$$\begin{aligned} \mathbf{d}L_f h_1 &= \mathbf{d}\left(\begin{bmatrix} 0 & -\frac{\mu}{m} & -\frac{u}{m} \end{bmatrix} \begin{bmatrix} 0 \\ -g\sin(\theta) - \frac{\mu}{m}u \\ 0 \end{bmatrix} \right) \\ &= \begin{bmatrix} g\cos(\theta)\frac{\mu}{m} & \left(\frac{\mu}{m}\right)^2 & \left(\frac{g\sin(\theta)}{m} + \frac{2\mu u}{m^2}\right) \end{bmatrix}. \end{aligned} \tag{S7}$$

We use a the second-order Lie derivative of $\mathbf{f}(\mathbf{x})$ to find a final vector

$$\begin{aligned} \mathbf{d}L_f L_f h_1 &= \mathbf{d}\left(\begin{bmatrix} g\cos(\theta)\frac{\mu}{m} & \left(\frac{\mu}{m}\right)^2 & \frac{g\sin(\theta)}{m} + \frac{2\mu u}{m^2} \end{bmatrix} \begin{bmatrix} 0 \\ -g\sin(\theta) - \frac{\mu}{m}u \\ 0 \end{bmatrix} \right) \\ &= \begin{bmatrix} -g\cos(\theta)\left(\frac{\mu}{m}\right)^2 & -\left(\frac{\mu}{m}\right)^3 & \left(\frac{-2\mu g\sin(\theta)}{m^2} - \frac{3\mu^2 u}{m^3}\right) \end{bmatrix}. \end{aligned} \tag{S8}$$

We can combine the vectors (S6), (S7) and (S8) into an observability matrix $\mathbf{O}_M$ for the

longitudinal state

$$\mathbf{O}_M = \begin{bmatrix} 0 & \frac{-\mu}{m} & \frac{-\mu}{m} \\ g\cos(\theta)\frac{\mu}{m} & \left(\frac{\mu}{m}\right)^2 & \frac{g\sin(\theta)}{m} + \frac{2/muu}{m^2} \\ -g\cos(\theta)\left(\frac{\mu}{m}\right)^2 & -\left(\frac{\mu}{m}\right)^3 & \frac{-2/mug\sin(\theta)}{m^2} - \frac{3/mu^2u}{m^3} \end{bmatrix}$$

The determinate of $\mathbf{O}_M$ is

$$|\mathbf{O}_M| = -\frac{u\cos(\theta)\mu^4 g + \sin(\theta)m\mu^3 g^2}{m^5}.$$

Since $\mu \neq 0$, the system will be locally observable except when

$$0 = -g\sin(\theta) - \frac{\mu}{m}u. \tag{S9}$$

We note that S9 is exactly equal to (11) when $\dot{u} = 0$. Consequently, the condition (S9) will only be true during unaccelerated flight, as it is then impossible to tell the difference between θ and u, making the state unobservable. Therefore, we may say that the longitudinal state $\mathbf{x}$ is locally observable during accelerated, $\dot{u} \neq 0$, flight. The ability to estimate the drag coefficient μ in the state of the vehicle, using only IMU measurements, makes it straightforward to use the drag-force enhanced model for quadrotor state estimation.

Author Information

Robert Leishman is a PhD candidate in the Department of Mechanical Engineering at Brigham Young University (BYU) and a recipient of the U.S. Department of Defense Science, Math, and Research for Transformation (SMART) Scholarship. Upon completion of his Ph.D. degree, he will work as a research engineer for the U.S. Air Force Research Laboratory. Robert received the B.S. degree in mechanical engineering from Utah State University in 2006. He was awarded a U.S. Air Force PALACE Acquire Scholarship through the Munitions Directorate at Hill Air Force Base, with which he received the M.S. degree in mechanical engineering from BYU. Robert is a student member of IEEE and AIAA.

Contact Information for the corresponding author:

rleish@gmail.com

Dept. of Mechanical Engineering

Attn: Robert Leishman

435 CTB Brigham Young University

Provo, UT 84602

John C. Macdonald Jr. received the B.S. degree in electrical engineering from Brigham Young University in 2002, the M.S. degree in electrical engineering from the Air Force Institute of Technology in 2006, and the Ph.D. degree in electrical engineering from Brigham Young University in 2012. Since February 2013 he has been a research electronics engineer in the United States Air Force Research Lab, Sensors Directorate.

Randal W. Beard received the B.S. degree in electrical engineering from the University of Utah, Salt Lake City in 1991, the M.S. degree in electrical engineering in 1993, the M.S. degree in mathematics in 1994, and the Ph.D. degree in electrical engineering in 1995, all from Rensselaer Polytechnic Institute, Troy, NY. Since 1996, he has been with the Electrical and Computer Engineering Department at Brigham Young University, Provo, UT, where he is currently a professor. In 1997 and 1998, he was a Summer Faculty Fellow at the Jet Propulsion Laboratory, California Institute of Technology, Pasadena, CA. In 2006 and 2007 he was a visiting research fellow at the Air Force Research Laboratory, Munitions Directorate, Eglin AFB, FL. His primary research focus is autonomous control of miniature air vehicles and multivehicle coordination and control. He is a past associate editor for the IEEE Control Systems Magazine and the Journal of Intelligent and Robotic Systems, and is currently an associate editor of the IEEE Transactions on Automatic Control.

Tim McLain is a professor in the Department of Mechanical Engineering at Brigham Young University (BYU) where he currently holds the position of department chair. He received BS and MS degrees in mechanical engineering from BYU. While completing his PhD work at Stanford University, Professor McLain worked with the Monterey Bay Aquarium Research Institute on the control of underwater robotic vehicles. He joined BYU in 1995. During the summers of 1999 and 2000, he was a visiting scientist at the Air Force Research Laboratory where he initiated research on unmanned aircraft an area on which he continues to focus. With Randy Beard, he is the author of the textbook Small Unmanned Aircraft: Theory and Practice published in 2012 by Princeton University Press. He is currently the director of the Center for Unmanned Aircraft Systems under the National Science Foundation Industry/University Cooperative Research Center program. Professor McLain is a senior member of IEEE, an

associate fellow of AIAA, and has served as a member of the AIAA Unmanned Systems Program Committee.